Journal of Engineering Science and Technology
Vol. 18, No. 1 (2023) 792 - 813

BEHAVIOR OF HIGH-PERFORMANCE REINFORCED ARCHED-HYBRID SELF-COMPACTING CONCRETE DEEP BEAMS

QASIM M. SHAKIR*, HAWRAA K. HANOON

Civil Engineering Department, University of Kufa, Najaf, Iraq
*Corresponding Author: qasimm.alabbasi@uokufa.edu.iq

Abstract

In the present work, a new model of hybrid deep beams has been presented. The proposed model is based on the curved distribution of concrete types along the beam rather than the conventional hybrid model. Then, the highly cost (steel fiber concrete) is used within the regions of high concentration of stresses only, resulting in minimizing the total cost of the beam. Six specimens of deep beams have been tested under static loads applied in two arrangement, one and two point loads. The behavior has been tracked in terms of the cracking and failure loads, the rate of crack propagation; horizontally and vertically, the loading history, crack width, toughness, stiffness and ductility. Results revealed that for the conventional hybrid model, capacity improved by 23% and 27% for the two loading systems respectively. The respective values for the proposed arched hybrid model are 23% and 32%. Moreover, Toughness enhanced by 44.7% and 143.7% for the conventional hybrid model. Whereas the improvements for the arched hybrid model, the respective values are 65.5% and 144.3% relative to the control beams, referring to relatively highly ductile behavior with using two-point load system and the arched hybrid model. Furthermore, ductility enhanced by 11.5% and 32.5% for the horizontal hybridization, against 12% and 37.4% for the arched model of hybridization.

Keywords: Deep beams, Ductility, Flexural and diagonal cracks, Hybrid deep beams, Light-weight concrete, Steel fibres reinforced concrete.

1. Introduction

ACI 318-19 building code [1] defined the Reinforced concrete deep beam as " members that are loaded on one face and supported on the opposite face and that clear span does not exceed four times the overall member depth *h*, or there is a concentrated load exist within a distance 2*h* from the face of the support". Deep beams are used as transfer beams in high-rise building, column-bearing beams, bridges, tank walls and foundation [2]. The load is transferred in deep beams through the strut-like compression elements can develop between the loads and supports [3]. Moreover, deep beams can be considered as one of the D-regions that strain distribution is no longer considered linear, and the shear deformations become significant when compared to pure flexure. Structural members, may include D-regions such as dapped-end beams [4], corbels [5], deep beams [6], openings in beams [7], etc. Such region may not yet, be studied using the (Bernoulli) theory [8]. Figure 1 shows some types of D-regions. Several approaches were proposed to consider such regions such as shear friction method [9] and Strut-Tie models STM [10].

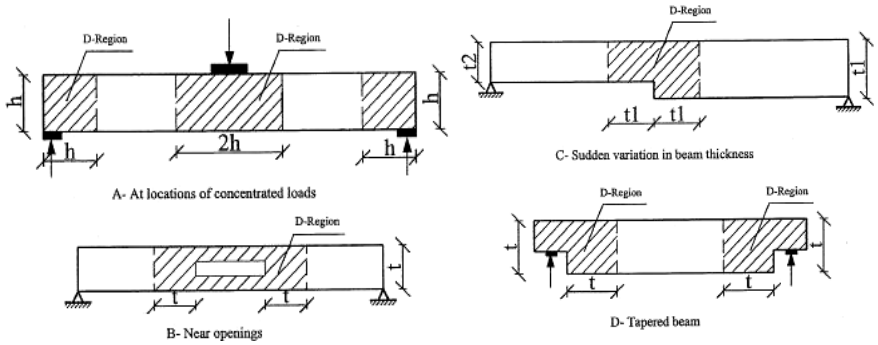

Fig. 1. D-regions in structural members.

Because of the large weight of deep beams, many researchers proposed different solutions to control this problem. One of these suggestions was introducing web openings by different sizes and shapes. Such proposal may not result in reducing beam weight only. But openings may be used for the passage of services of the building. However, It was reported that inclusion web opening may result in a drop of beam capacity, especially for opening that lie along the compression struts of the beam. Amongst studies in this regard were achieved by Chine and Doh [11] about deep with opening. Shape of opening and shear span to overall depth ratio (a/h) were the controlling variables. It was found that circular and square openings reduced the capacity by (30-35)% and (40-80)% respectively.

In order to improve the behavior of deep beams containing opening, openings were strengthened by various means, including the reinforcing around openings, addition of steel fibers, using CFRP composites etc. Ibrahim et al. [12] tested the efficiency of two steel reinforcement configurations around openings located at the shear spans. The first one included using reinforcement along the struts. While the other included using vertical and horizontal reinforcement. It was reported that adding reinforcement around the openings improved the load capacity by (23-50) %, or around opening only, Hamad and Shakir [13] investigated reinforced concrete deep beams strengthened with different techniques in the opening zone. The

strengthening of openings with different proposals improved the load capacity. The increment in the load capacity for beams was about (8.5 to 21.37%) compared to the control beam. Punnoose and Hameed [14] reported that the presence of the openings in the shear span region has a greater impact on the capacity of the beam, and if it is outside it, the deep beam behaves in a manner similar to the solid deep beam. Saeed and Yousif [15] studied steel fibrous continuous deep beams with and without openings. Shakir et al. [16] used CFRP in strengthening the regions around the large opening in T-deep beams. Rahim et al. [17] considered deep beams with square openings strengthened with CFRP.

Consequently, high content of steel fibers is used to affect shear strength. Thus, cost may increase and some problems in casting the concrete may occur. To reduce weight, Light weight concrete was used in a few studies, Ali and Lazim [18] studied the behavior of lightweight concrete deep beams. It was concluded that the use of lightweight concrete instead of normal weight concrete reduces the first diagonal cracking and ultimate load. The reactive powder concrete (RPC) was used in some studies about deep beams to improve the general performance of such members but little research has studied it because of its high cost. Fahmi et al. [19] investigated the behavior and shear strength for deep beam made of reactive powders concrete, the effects of shear span to effective depth ratio (1,1.25,1.5,2) and found that when the shear span to effective depth ratio is low from 1.5 to 1.25 and 1, the ultimate shear strength increased by 24.4% and 31.7%, respectively.

However, the high cost restricts adopting such proposal widely. In this regard, Hasan and Al-Shamaa [20] added air bubbles in the lower half of reactive powder concrete deep beams. It was reported that the use of bubbles in one and two layers reduced the weight of the beam by (9-13)% and (19-26)%. Capacity reduced by (7-13)% and (12-22)% respectively. Lateef and Ahmed [21] considered reactive powder concrete deep beam. The variables discussed were the width of the deep beam and the type of concrete, after the examination, results revealed that the width increase from 150 to 200 mm increases the ultimate strength by 13.04% and 18.7%, for normal and Ultra-High Performance concrete respectively.

The hybrid type of deep beams was considered in several studies. In this model, high strength concrete was used within the upper part of the beam and normal strength concrete (or lightweight concrete) is used within the lower part. Hassan [22] tested hybrid deep beams of the two layers of concrete (ultra-high performance concrete UHPC and normal concrete). UHPC used was compression in the hybrid beams. Results showed that the capacity of beam increased by increasing the thickness of the UHPC layer and the proportion of steel fibers used in concrete. Hassan and Faroun [23] studied the hybrid deep beams, two types of concrete were used, where fibrous concrete was placed on both sides of the beam in the shear span area, and in the middle was normal concrete. It was observed that the ultimate load rate in the case of repeated load decreases by (27.08% and 25.09%) when the ratio of fibers is 1% and 2%, respectively, decreases by (20.81% and 18.81%) when the case of normal concrete and fibrous concrete, respectively.

Sada and Resan [24] used the trapezoidal section with side angle (75°, 80°, 85°), for deep beams instead on the rectangular. It was reported that the ductility of hybrid trapezoidal deep beams was improved compared to the rectangular section. As the deep beam is of the D-region type, thus, high disturbance of stresses within supports exists. Consequently, using NSC or LWC within the lower part of the

beam may result in premature failure or the anchorage ends (for lightweight concrete) may not provide sufficient strength to develop the required tie force.

This work presented a new model of hybrid deep beams that is incorporated the mechanisms of the tied arch and arch action. The proposed model, which is adopted, the curved distribution of the two types of concrete, is based on the STM models. In this model, the high performance concrete is used within the compression struts and the region of high concentration of stresses (supports).The aim of the proposed type of hybridization (in its full project) is to produce deep beams that qualify the requirements of high strength, low cost and weight. It is also, may be extended to produce sustainable deep beams that incorporate the recycled aggregate within concrete out of the path of stress transfer.

2. Experimental Program

2.1. Description of specimens

Six self-compacting deep beams, with a cross section of 450 mm total depth, 180 mm width and a total length of 1700 mm, three are tested under two point loads with a shear span/depth ratio of $a/h = 1.2$, and the other is tested under the influence of one point load at mid span as shown in Fig. 2.

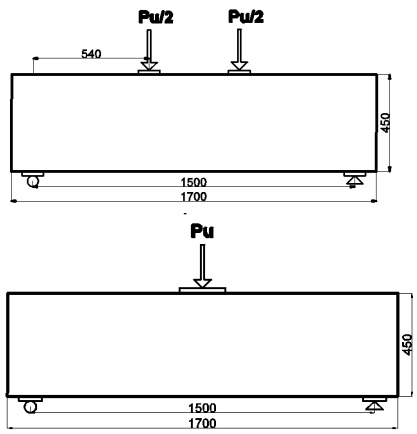

Fig. 2. Loading setup of the deep beam(Units in mm).

The study consists of two specimens of normal self-compacting deep beams, as a reference, two models of horizontal hybrid self-compacting deep beams in first group G1, the concrete is a high strength (steel fibers concrete) in the upper half of the beam and a self-compacting concrete in the lower half. The second group G2 consists of two specimens of arched hybrid self-compacting deep beams. The concrete is a high strength (steel fibers concrete) in the strut's region of the beam and a lightweight concrete in the tie region Figs. 3(a) and (b) show the geometry of G1 and G2. Steel reinforcement was designed based on the strut and tie model (STM) according ACI318M-19 [1] ,where steel reinforcement consisted of (3Ø16 mm) bars as longitudinal reinforcement, (2Ø10 mm) bars were used in the compression region and (Ø8 @130mm C/C) were used as shear reinforcement as shown in Fig. 3(c). Table 1 shows the coding and details of the tested specimens.

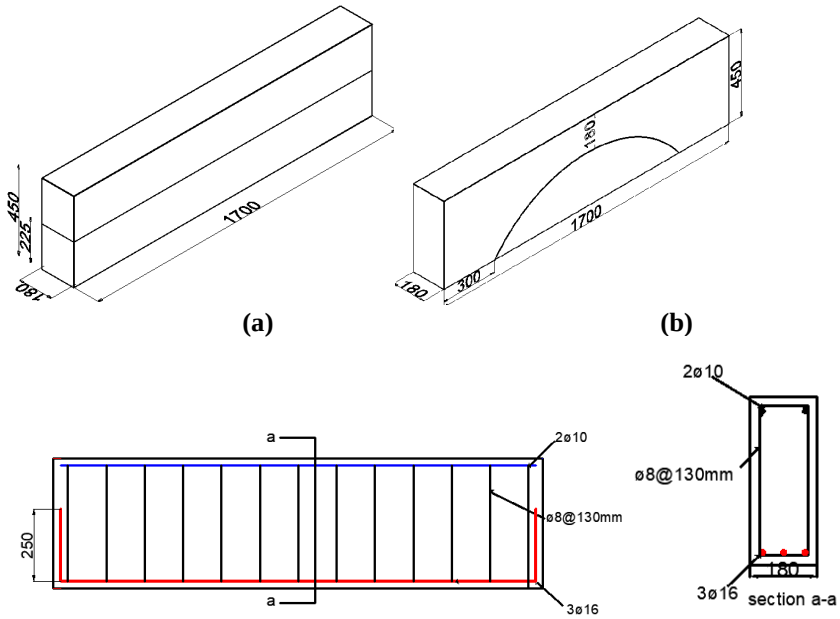

Fig. 3. Details of the tested deep beams (All units in mm).
(a) Horizontal hybrid beam (b) Arched hybrid beam(c) Reinforcement.

Table 1. Coding and details of deep beams.

Coding	*a/h*	Geometry of deep beam
CTRL-1P	1.67	Not hybrid
CTRL-2P	1.2	Not hybrid
G1-SN-1P	1.67	Horizontal Hybrid, Fig. 3(a)
G1-SN-2P	1.2	Horizontal Hybrid, Fig. 3(a)
G2-SL-1P	1.67	Arched Hybrid, Fig. 3(b)
G2-SL-2P	1.2	Arched Hybrid, Fig. 3(b)

Note**:**1P**: o**ne point loading; 2P: two point loading

2.2. Materials and fresh concrete tests

The constituent materials of mixes were ordinary Portland cement (CAR) that has been tested to qualify the requirement of IQS. No.5, 1984 [25]. Washed natural sand, natural crushed gravel that are tested according to IQS. No. 45/1984 [26]. In Normal and steel fiber concrete (SFC), gravel with maximum sizes of 19 mm and 14 mm are used. Light weight gravel (Leca) has been used in lightweight concrete mix having a max size (8mm). Straight micro steel fibers with diameter of 0.22 mm and length 13.1 mm have been used with 1.5% by weight for the purpose of enhancing the shear resistance and improving the durability of the SFC mixes. Its tests complied with the requirements of ASTM A820-06 [27]. Three different sizes of steel reinforcement have been used. Teste are achieved in the Construction Laboratory of the University of Kufa, according to ASTM A615 [28] as shown in Table 2. Master Glenium 54 has been used in concrete mixtures to produce the mixture self-compacting and reduce the percentage of water. Properties are provided by manufacturer and checked to qualify the requirements of ASTM C-

494 Type F & G BS EN 934-2 [29]. Limestone which is known locally as (Al-Gubra) that has been used as filler material in self - compacting concrete. Table 3 shows the mixing ratios of the types of concrete used.

Self-consolidating concrete (SSC) tests have been carried out on normal and lightweight concrete to ensure that it comply with the requirements of the fresh SSC mix. Slump flow and T500 Tests to estimate the flow ability of self-compacting concrete according to the ACI 237R-07 [30], J-ring Test to test the passing ability of self-compacting concrete ASTM (C1621/C1621M) [31]. The test results are listed in Table 4.

Table 2. Properties of steel reinforcement bars.

Nominal diameter	Yield stress (MPa)	Tensile strength (MPa)	Elongation %
8	445	630	13.22
10	480	695	13.63
16	600	697	15.7

Table 3. mixing ratios of concrete.

Materials	SFC	LWC	NC
Cement (kg/m^3)	517	400	470
Sand (kg/m^3)	600	650	837
Gravel (kg/m^3)			800
Gravel 14mm (kg/m^3)	1122		
L W A (Leca) (kg/m^3)	-	400	-
Steel fiber (kg/m^3)	117	-	-
Silica fume(kg/m^3	-	8	-
Limestone(kg/m^3)	-	-	99
Water(l/m^3)	165.4	146.88	159.32
Super plasticizer(l/m^3)	3.88	6.53	7.52

Table 4. Results of the SCC tests.

Test	Result		Specification limit
	NC	LWC	
Slump flow (mm)	630	720	450-760
T500 (s)	3	3	3-5
J-ring (mm)	35	37	25-50

2.3. Casting and tests of hardened concrete

The forms were made of plywood and the steel plate separating the two types of concrete was fixed inside the forms after installing the steel cage in place, as shown in the Fig. 4. Two types of concrete were mixed at the same time using two mechanical mixers and casting into the mold, the steel plate was removed immediately after casting. At the same time. Three cylinders (150 mm diameter, 300 mm length) to check compressive strength (f 'c) according to ASTM C39/ C39-15a [32], three cubes (100 X 100 X 100) mm were sampled to check the compressive strength (f_{cu}) according to BS 1881-116 1983 [33], and three cylinders (100 mm diameter, 200 mm length) to test splitting tensile strength ASTM C496 -11 [34]. Moreover, cylinders (150 mm diameter,

300 mm length) were sampled to find the modulus of elasticity ASTM C496-14 [35]. All samples were tested at the age of 28 day.

(a) **(b)**

Fig. 4. Formwork and casting of hybrid beams (a) horizontal, (b) arched.

The tests are shown in Fig. 5. Table 5 shows the results of tests for the various concrete mixes. After the initial hardening and the removal of the moulds, the curing began with warm water and the beams are covered with burlap sacks and plastic sheet to maintain humidity and temperature. The stress - strain curves for the concrete types used and reinforcing steel used in the present work are shown in Fig. 6.

(a) **(b)** **(c)** **(d)**

Fig. 5. Mechanical properties of hardened concrete (a) Cylinder test (f'c) (b) Cube tests (c) Tensile Splitting Test (d) modulus of elasticity.

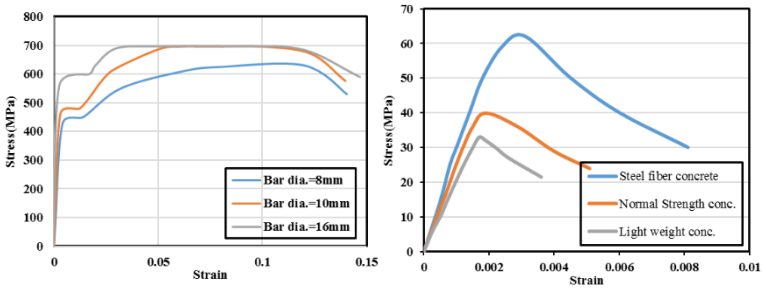

(a) Reinforcing steel **(b) Concrete**

Fig. 6. Stress-strain curves for concrete and reinforcing steel.

Table 5. Results of the mechanical properties of hardened concrete.

Type of mix	Cube compressive strength MPa (f_{cu})	Cylinder compressive strength MPa(f `c)	Splitting tensile strength MPa (f_t)	Modulus of elasticity GPa (E)	Density kg/m^3
SFC	72	62	7.72	34.8	2538
NC	46	39	2.41	26.9	2400
LWC	37	32	2.28	23.2	1830

2.4. Instrumentation and testing machine

The deflection of the deep beam was measured at two points, mid- and quarter-face of the beam, using (LVDT) as shown in Fig. 7(a). The crack width was measured using a crack meter with a range of 0.5 mm. When the crack width exceeded 0.5 mm, the crack was measured with a digital Vernia. Every 20 kN, the crack width was measured. Figure 7(b) shows the crack meter and Vernia. Furthermore, the data logger device was used to record the load deflection data as shown in Fig. 7(c). The universal test machine of 2000 kN, shown in Fig. 8 is used to test reinforced concrete deep beams

(a) **(b)** **(c)**

Fig. 7. (a) LVDT (b) Crack meter and Vernia (c) Data logger.

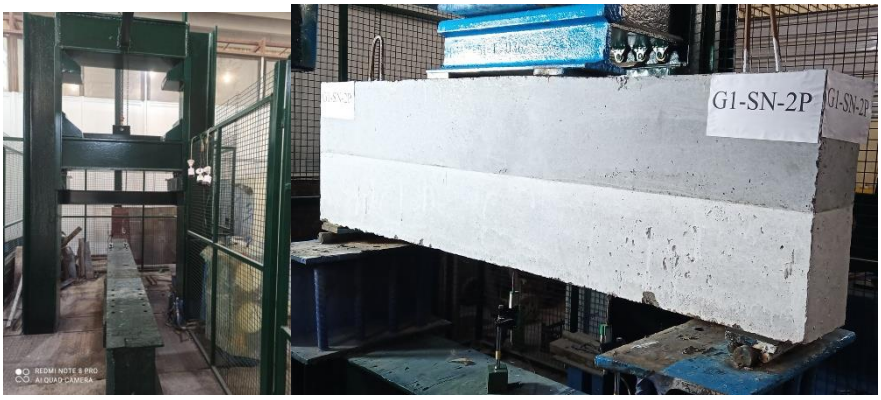

Fig. 8. Loading machine and testing.

3. Test Results

3.1. Crack patterns at failure

A. CTRL-1P Specimen

Figure 9(a) shows crack pattern which shows that the first crack initiated as a flexural crack at mid span within load of 70 kN. This may be attributed to the profile of bending moment diagram which reveals that maximum moment (PL/4) occurred at mid span, and due to the low tensile strength of concrete at bottom face. With further loading, cracks propagated on both sides of the beam with smaller slope due to the interaction between the decreased bending moment (B.M) and the constant shear force (at the shear span). At a load level of 160 kN, the outermost diagonal crack that is proposed to connect the point load with support initiated. It seems that this crack does not lie within the compression strut exactly because that the flexural mode of failure controlled the response of the final stage of loading. Besides, cracks developed up towards the compression face resulting in gradual diminishing in the compression block up to the level of 410 kN at which failure occurred. No crushing at the compression face has been observed. Thus, it can be concluded that higher capacity can be obtained if the tensile steel is increased. It is to be mentioned that some crushing occurred in the support regions due to the high concentration of stresses. It can be seen that the control beam, that was designed by STM models showed ductile behaviour and the mode of failure is shifted from being diagonal to be of the flexural type.

B. G1-SN-1P Specimen

Figure 9(b) shows the map of crack propagation at failure, where the first crack initiated at load 80 kN as a flexural crack at the mid span where maximum moment occurred. With progressive loading, the crack developed vertically up to reaching the layer of steel fiber concrete. Then, the propagation of cracks is slowed down. Consequently, more cracks spread horizontally towards the supports with angles from horizontal decreases away from the flexural crack. Shear cracks ascend diagonally towards the loading point. However, the development of most cracks is restricted within the top layer preventing formation of actual diagonal cracks around or along the compression struts. Thus, the first flexural crack developed vertically to the loading point, and most of the strain energy was dissipated in. Some crushing occurred at the support reactions (D-regions) due to the relative high concentration of stresses. The failure occurred at 460 kN load by flexural mode. Compared to the reference specimens CTRL-1P, the capacity of the hybrid deep beam increased by 12.2%.

C. G2-SL-1P Specimen

For this model, in which cracking pattern is shown Fig. 9(c), the arrangement of the concrete types was hybridized that the high-strength concrete (steel fiber concrete) was used in the strut and the support area, and light weight concrete in the region. The first crack appeared as a flexural crack area at a load of 80 kN. Beyond this stage, more cracks developed on both sides and spread within the shear span zones resulting in the appearance of some diagonal cracks at 120 kN. The rate of propagation of cracks within the lightweight concrete would be relatively high in both horizontal direction (in terms of development more cracks) and vertically (in terms of

penetration through the depth of the section). However, the rate of development diminished while penetrating through the region of steel fiber concrete. Consequently the diagonal cracking developed mostly in the lightweight concrete region. Therefore, no diagonal crack developed along the compression struts which represent the most likely paths of failure for deep beams. Also, no crushing occurred at supports due to the high compressive strength of concrete that the D-region may accommodate relatively higher stresses if compared with the specimens CTRL-1P and G1-SN-1P. It is to be mentioned that no crushing occurred at the compression face under the point load revealing that higher capacity may be gained by controlling the widening of the flexural crack at mid span. Failure occurred at load level of 502 kN following flexural mode of failure. Improvement in capacity was obtained of 22.4% and 9.1% compared with CTRL-1P and G1-SN-1P specimens respectively.

D. CTRL-2P specimen

The map of cracking propagation the specimen is shown in Fig. 9(d). As usual, the first crack occurred at mid span within the region of pure bending moment (B.M). With progress in loading, no further cracks occurred at this region up to the load of 120 kN at which vertical cracks developed at the junction of the maximum B.M and the maximum shear regions. More cracks developed on both sides towards the supports following paths of a gradually decreased angles. At a load level of 200 kN, the diagonal crack along the compression struts developed. However, some crushing near support occurred before failure. At a load level of 400 kN, some horizontal cracking occurred at the compression face revealing that there is some tendency for spalling of concrete may occur if higher ratio of main steel is used. The beam failed at load of 542 kN following a diagonal (flexural-shear) mode of failure.

E. G1-SN-2P Specimen:

The first crack developed at the region of maximum moment within the load of 80 kN Fig. 9(e). Diagonal crack initiated at 160 kN with angle from horizontal more than the G1-SN-1P model. Under further loading, the cracks grow to the top and slow down when it reaches the high strength concrete. When the loading reaches 688 kN, the model failed by shear-flexural (diagonal) cracking. It can be observed that adopting the horizontal configuration of hybrid concrete deep beams resulted in enhancement in the capacity of deep beam by 26.9% compared with control specimens CTRL-2P.

F. G2-SL-2P Specimen

This specimen is similar to specimen G2-SL-1P but it tested under two-point loads. Figure 9(f) shows the development of cracks on the sample throughout the loading process. The first crack appeared in the flexural area with loading 60 kN and at the shear area 80 kN. The cracks spread rapidly within the region of the lightweight concrete. The rate of development was restricted considerably within the high strength concrete. Thus, no crack is observed to develop near the supports nor fully diagonal crack developed as in specimen CTRL-2P. Furthermore, no crushing occurred at the compression face nor close to the supports. Such type of cracking distribution is favourable when it is intended to repair or to strengthen the specimen. When the load reaches 717 kN, the specimens failed following a flexural mode of failure. It can be observed that the capacity improved by 32.3% compared to the reference specimen CTRL-2P. Table 6 shows the tests result of specimens.

Table 6. Experimental test results of specimens.

Specimens	Cracking load p_{cr}(kN)	Ultimate load pu (kN)	Max. deflection (mm)	Max. crack width (mm)	Mode of failure
CTRL-1P	70	410	13.8	3.05	Flexural-shear failure
CTRL-2P	80	542	12.23	2.64	Flexural-shear failure
G1-SN-1P	80	460	15.27	3.5	Semi-flexural failure
G1-SN-2P	80	688	22.01	1.45	Flexural-shear failure
G2-SL-1P	80	502	18.36	2.4	Flexural failure
G2-SL-2P	60	717	21.2	3.94	Flexural failure

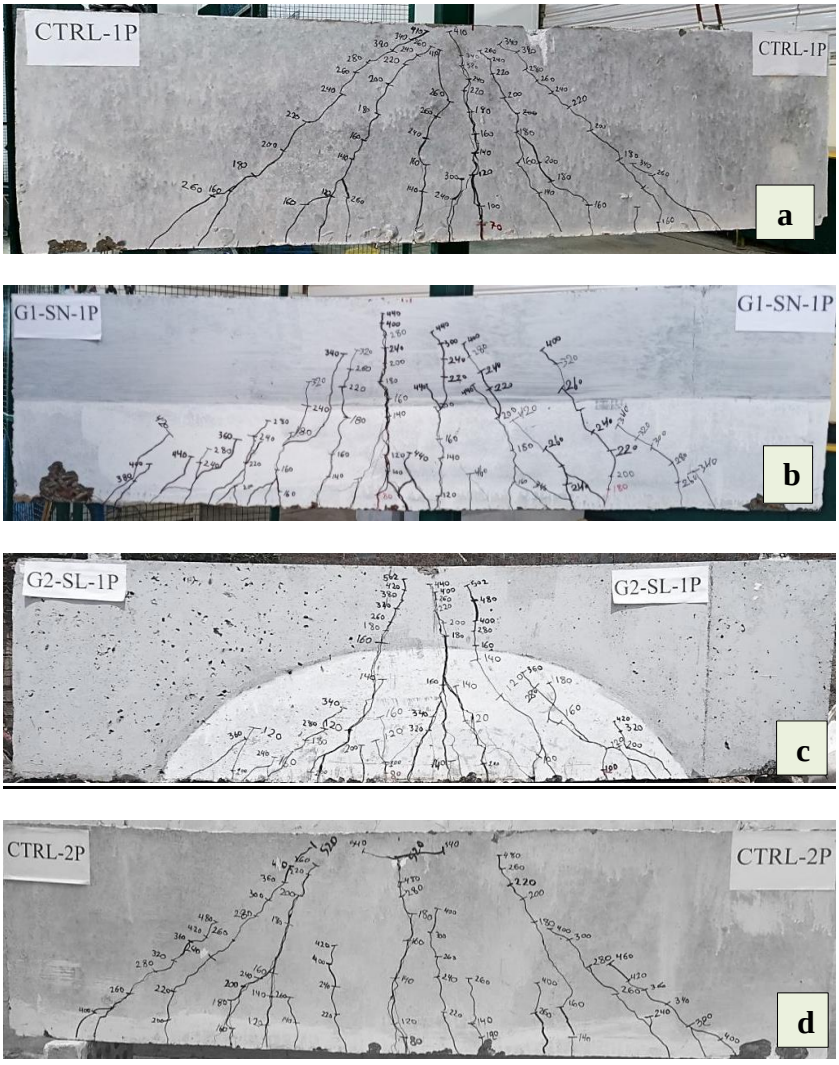

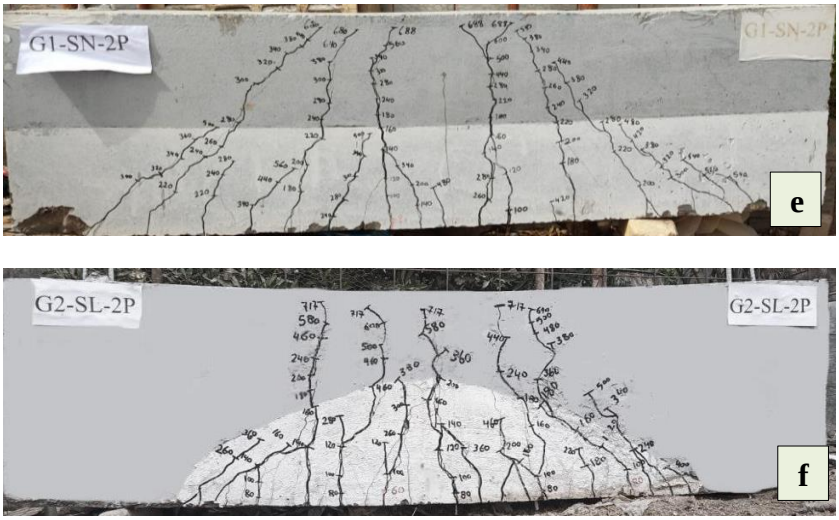

Fig. 9. Crack patterns for the tested specimens.
(a) CTRL-1P, (b) G1-SN-1P, (c) G2-SL-1P,
(d) CTRL-2P, (e) G1-SN-2P, (f) G2-SL-2P.

3.2. Load- deflection curve

3.2.1. One point load

Figure 10(a) shows the load-deflection curve of specimens tested under one-point loading system. For the control specimen, the initial stiffness was 55 kN/mm which was kept constantly up to 350 kN. Then, it dropped to a value of 16 kN/mm and remained constant up to failure. The constant values of stiffness through the two parts (before and after 350 kN) reveal that the rate of transfer of stress from concrete to steel was uniform in general. Also, that the propagation through the concrete body occurred in two rates, one of low rate which is represented by the region around mid-span, and the outer zone which inclined to compression strut. The second was when cracking developed beyond the level of the neutral axis of the section.

For specimen G1-SN-1P, it can be seen that the initial stiffness was 65 kN/mm which was kept constantly up to 360 kN, as in the control specimen. Beyond which, gradual reduction in stiffness occurred due to the propagation of the cracks through the bottom normal strength concrete (NSC) layer. This rate of reduction increased slightly up to instant of failure, which occurs at level 460 kN.

For specimen G1-SL-1P. Some softening behavior can be noticed at an early stage of 15 kN. Then, the equilibrium was maintained again by an internal mechanism induced by (STM model), which kept the stiffness to be in a value of 63 kN/mm up to a load of 375 kN. After that, stiffness reduced again to a constant value of 10 kN/mm due to the propagation of cracking within the (LWC) part up to failure at 502 kN.

3.2.2. Two point loads

Figure 10(b) shows the load-deflection curve of specimens tested under the two-point loading system. It can be noticed that the stiffness of the reference specimen

CTRL-2P was almost constant with a value of 70 kN/mm until the loading reached 440 kN. Then, the slope of the load-deflection curve decreased and rapid increment in deflection relative to the applied load was observed to record a maximum deflection of 12.24 mm when loading 542 kN. It was found that the stiffness of this model increases by 25.45% compared to the CTRL-1P model.

For G1-SN-2P specimen, at the early stage of the loading deflection increased regularly and linearly with stiffness of 70 kN/mm This may be due to the uniformity of the distribution of cracks through the concrete. The rate of cracking propagation and reduction remained constant up to a load of 510 kN at which stiffness decreased to 22 kN/mm. However, stiffness decreased linearly through this stage up to the instant of failure at load 688 kN recording maximum deflection of 22 mm which is more than that for the control specimen by 79.8 %. Consequently, it is noted that the beam capacity increased by 26.9% compared to the reference model CTRL-2P.

G2-SL-2P shows slightly softening behavior up to a load of 180 kN. This behavior is due to the rapid spread of cracks throughout the lightweight concrete layer. When the cracks propagated in the high-strength concrete SFC, it begins to uniformly slow down, and the stiffness seems to be stable up to a load of 520 kN. After which the stiffness decreased to 20 kN/mm due to rapid widening of the flexural crack. The specimen begins to fail with a load of 717 kN, with a maximum deflection of 21.2 mm. It is noticed when using the arch model that it helped to increase the stiffness of the sample, it is to be mentioned that the beam capacity enhanced by 32.3 % relative to the control specimen.

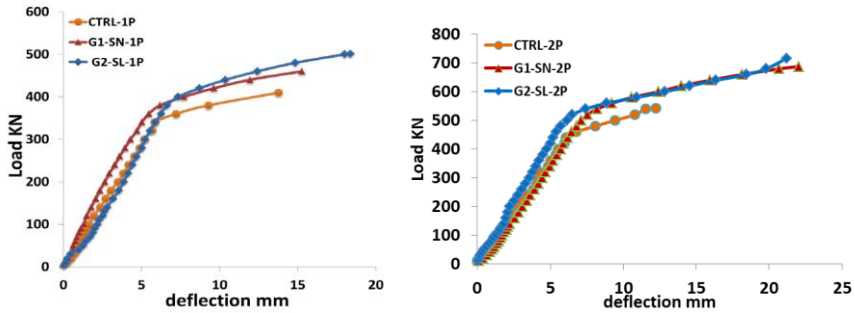

(a) **(b)**

Fig. 10. Load-deflection curves (a) one point load (b) two point loads.

3.3. Crack width

For the control specimen CTRL-1P, the width of the flexural and diagonal cracks increased in a uniform similar rate up to a load of 300 kN. After that, the flexural crack begins to develop as the dominant crack with width of 3.05 mm at maximum load, while the width of the diagonal crack is 1.1 mm. This refers that the failure occurred is by flexural mode. For G1-SN-1P specimen, the flexural cracks appeared first at a load of 80 kN. Then, the diagonal cracks appeared at 180 kN. The rate of widening of the two cracks was in equilibrium up to a load of 350 kN. Then, the flexural crack begins to develop rapidly, because that the diagonal crack has been restricted when reaching the steel fiber concrete (SFC) layer. The upward vertical crack developed towards the loading point and becomes dominant with maximum width of 3.5 mm and 0.45 mm for the diagonal shear crack. For specimen G2-SL-1P

specimen, despite the dominance of flexural failure, the flexural and diagonal cracks are close together to the extent of 350 kN. The maximum crack width is less than the previous two models because of the existence of the steel fiber concrete, which is in an arc-shaped surrounding the weak area, resists the development of cracks. The measured flexural crack width was 2.4 mm while the diagonal crack 1.02 mm.

For specimen CTRL-2P, the rate of widening of the flexural and diagonal was the same up to load level of 460 kN. When the specimen loaded close to failure, the width of the flexural crack begins to develop rapidly, reaching a maximum width of 2.64 mm at loading 542 kN, and the width of the diagonal crack width is 1.82 mm. For specimen G1-SN-2P, the width of the two types of cracks is close to other up to 510 kN, Beyond which, the flexural crack increased slightly relative to the diagonal crack. The maximum width of the cracks were 1.45 mm and 1.12 mm for flexural and diagonal crack, respectively. For G2-SL-2P specimen, the flexural crack is dominant because it is located within lightweight concrete, where the crack width is 3.94 mm. While the width of diagonal crack was 1.03 mm and has a slight slope closer to region of maximum bending moment. Figure 11 shows the measured crack widths with load application for the tested specimens. Knowing that "f" and "d" in legends refer to flexural and diagonal cracking respectively.

Table 7 shows the load deflection and crack width at service load.

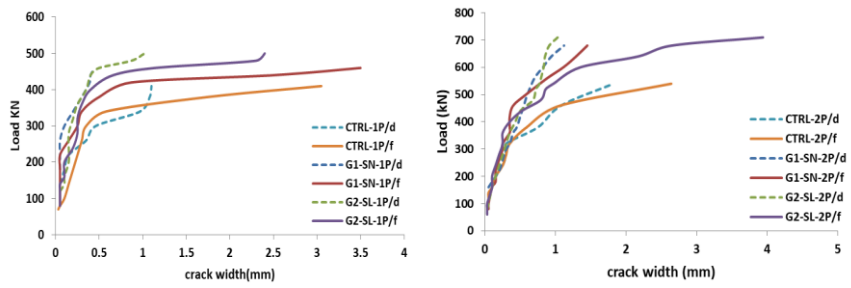

(a) **(b)**

Fig. 11. Crack width (a) one point load, (b) two point loads.

Table 7. the load deflection and the crack width at service load.

Specimen	CTRL-1P	G1-SN-1P	G2-SL-1P	CTRL-2P	G1-SN-2P	G2-SL-2P
Deflection (mm)	5.5	5.22	6.5	5.86	7.5	4.22
Crack width(mm)	0.46 d	0.3 f	0.35 f	0.93 d	0.85 f	0.75 f

3.4. The rate of cracks propagation

Figures 12(a) and (b) show the rate of crack propagation for the specimens tested under one point loading system in the vertical and horizontal direction respectively. For Fig. 12(a) , it can be seen for the three specimens that the rate very high up to a load of 250 kN which penetrated about 400 mm of the depth of the section. Beyond which, the crack development slowed down consider due to the effect of the compression force on the top fiber, up to reaching failure.

For Fig. 12(b) that showing the rate of spreading of cracks horizontally towards to the supports, it can be seen that for the control specimen the propagation was generally uniform and rapid with load increment and that the diagonal crack development (at 650 mm) for the centre line. For the hybrid beam G1-SN-1P, the rate is similar to that the control specimen up to 250 kN at which the diagonal crack developed at distance 680 mm from mid span. Then, it developed rapidly towards the point load. For specimen G2-SL-1P, it can be seen that the crack development was very high up to a load of 150 kN which reached at distance 300mm from the centre line. Beyond which, the horizontal propagation was slowed down because of the steel fiber concrete layer at the two supports which restricted the excessive curvature of the beam.

The diagonal crack developed at load at 350 kN at a distance of 420 mm from the mid span. This reveals that both the control and the conventionally hybrid deep beams had a tendency to fail by the diagonal mode more than the flexural mode. While the proposed hybrid deep beam had a clear tendency to fail by the flexural mode. This may be expressed in terms of ductile behavior, that more ductile behavior can be expected for the proposed hybrid deep beam if compared with other two beams.

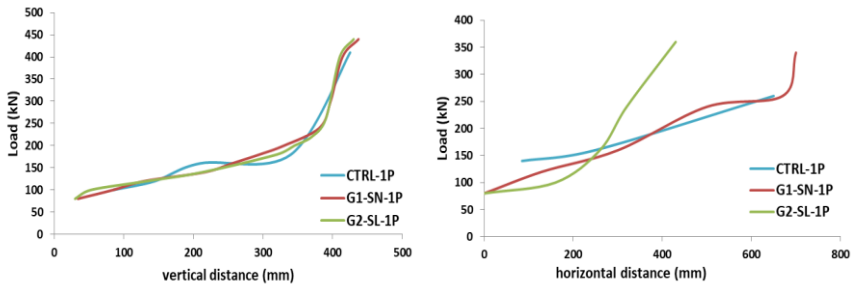

(a) **(b)**

Fig. 12. Crack propagation of one point load (a) vertical, (b) horizontal direction.

For specimens tested under two point loads, the diagram of spreading of cracks in the vertical direction shown in Fig. 13(a), similar rate of propagation can be observed for all specimens until the load reaches 160 kN, with a depth of 220 mm. Then, the rate is slowed down for the hybrid deep beams due to the presence of fibrous concrete, which resists crack propagation. The rate of crack propagation in the horizontal direction is shown in Fig. 13(b). Before loading reaches 200 kN, all of the three specimens reaches a distance of 400 mm from the mid span of the beam, after which the control specimen CTRL-2P begins to spread horizontally by looking and reaches close to the supports at a distance of 680 mm with a load of 400 kN. As for the G1-SN-2P specimen, the approach of cracks to the supports is slower so that it reaches 700 mm and its load 520 kN. Whereas in the hybrid model G2-SL-2P, the cracks are confined within the lightweight concrete without reaching steel fiber concrete and remain within the limits of 510 mm from the middle of span with a loading of 400 kN.

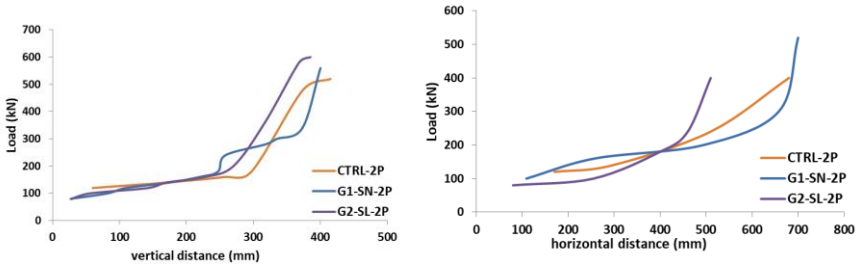

(a) **(b)**

Fig. 13. Crack propagation of two point load (a) vertical, (b) horizontal direction.

3.5. Flexural toughness

Toughness is a measure of a member's resistance to distortions prior to failure. The energy produced by the member is steadily lost up to failure by deformation causing cracking throughout the RC member, which is represented by the area under the curve [36-38]. Figure 13 shows the calculated toughness for the tested specimens. It can be seen that the reference CTRL-1P specimen has the lowest toughness, which is 3908 kN-mm. When using the steel fibers at the top layer for the horizontal hybrid G11-SN-1P, the toughness improved by 28%, Because that the steel fiber concrete which covers most of the strut's area improved the rigidity of beam significantly. For specimen G2-SL-1P, toughness improved by 65.5% compared to the reference model. In the case of two-point load, the enhancement in toughness was more evident, as the toughness of the reference model CTRL-2P was 4413 kN-mm. While for G1-SN-2P specimen recording enhancement by 143.7%, and almost it is very close to the arched hybrid deep beam G2-SL-2P, which was 144.3%. Table 8 and Fig. 14 shows the results of toughness for specimens.

Table 8. Results of toughness for specimens.

Specimens	Toughness (kN*mm)	(ΔT)% Toughness Ratio
CTRL-1P	3908	
G1-SN-1P	5003	28
G2-SL-1P	6468	65.5
CTRL-2P	4413.3	
G1-SN-2P	10756	143.7
G2-SL-2P	10782	144.3

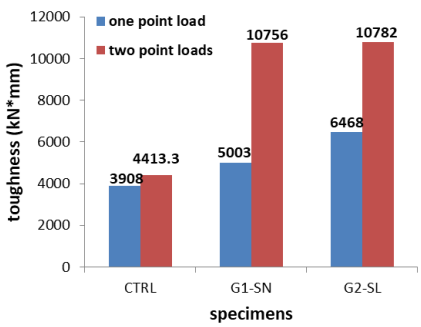

Fig. 14. Toughness for specimens.

3.6. Stiffness

The stiffness (K) is a measure of the resistance offered by an elastic body to deformation. The "effective secant stiffness" which is based on the strength at the service load stage (0.75*Pu) has been adopted [39]. Hence, the effective stiffness (Ke), can be estimated by using Eq. (1)

$$k_e=\frac{0.75Pu}{\Delta_{0.75\mathrm{Pu}}} \quad (1)$$

where K_e: effective stiffness , Pu: the ultimate load, $\Delta_{0.75Pu}$: the deflection that corresponds to the load level (0.75 Pu)

Table 9 shows the stiffness values of the tested deep beams. For one point load, it can be found that the value of stiffness for G1-SN-1P specimen increasing by 20% compared to the control specimens and G2-SL-1P specimen stiffness increased by 5.5% compared to the control specimens. It is to be mentioned that the reduction in stiffness of the specimen G2-SL-1P may be attributed to high ductility and that the plastic part (the second part of the load deflection curve) is larger relative to the specimen G1-SN- 1P. For two point load, the difference in values for the control and G1-SN-2P specimens was negligible, while the enhancement in stiffness for the G2-SL-2P model with 6.3% compared to CTRL-2P. Figure 15 shows the values of the effective stiffness for the tested specimens.

Table 9. Results of stiffness enhancement for specimens.

Specimen	0.75 Pu (kN)	Deflection at 0.75Pu (mm)	Stiffness, K (kN/mm)	ΔK%
CTRL-1P	307.5	5.7	55	
G1-SN-1P	345	5.22	66	20
G2-SL-1P	376.5	6.5	58	5.5
CTRL-2P	406.5	5.86	69.3	
G1-SN-2P	516	7.5	68.8	-0.8
G2-SL-2P	537.75	7.3	73.7	6.3

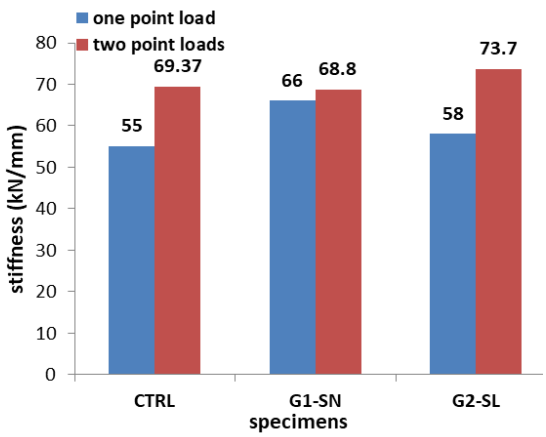

Fig. 15. Stiffness for specimens.

3.7. Ductility ratio

The ability to resist inelastic deformation without diminishing the ultimate load till failure is characterized as ductility [40, 41]. When the load at which steel gives is unknown, several ways have been proposed. A mothed that is adopted in the present work is based on the energy dissipation throughout the full history of loading and that within the elastic stage only, as shown in Fig. 16. Then, the ductility ratio can be expressed as:

$$\mu=0.5\left(\frac{E_{tot.}}{E_{el.}}+1\right) \quad (2)$$

where E_{tot} is the total energy dissipated up to failure, E_{el} is predicted energy dissipated within the elastic stage of loading only (area of the hatched triangle). The ductility ratio for the specimens shows in Table 10 and Fig. 17.

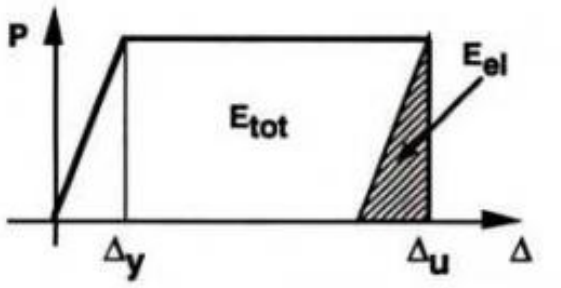

Fig. 16. Determination of ductility ratio by dissipated energy method [39].

Table 10. Results of ductility for specimens.

Specimens	E_{tot} (kN*mm)	$E_{el.}$ (kN*mm)	μ	Increasing in ductility%
CTRL-1P	3908	1465	1.83	
G1-SN-1P	5003	1725	1.95	6.6
G2-SL-1P	6468	2083	2.05	12
CTRL-2P	4413	1951	1.63	
G1-SN-2P	10756	3274	2.16	32.5
G2-SL-1P	10782	3097	2.24	37.4

Through the results, it was noted that the use of a layer of steel fibers in the upper half of the deep beam G1-SN-1P and G1-SL-2P specimens, increased the ductility by 6.6% and 12% respectively compared control specimen because the steel fibers increase the plasticity by keeping the concrete cohesion and bonding its particles as long as possible.

When two point loads were applied, the percentage of increase in ductility was gradual, as the ductility of the G1-SN-1P and G2-SL-1P specimens increased by 32.5% and 37.4% respectively compared with control specimens CTRL-2P.

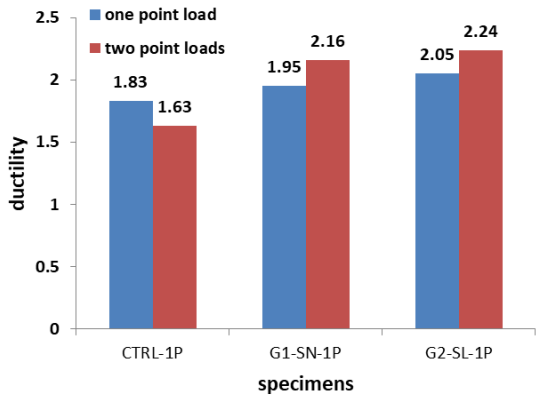

Fig. 17. Ductility for specimens.

4. Conclusions

In this study, the principle of hybrid beams was adopted to improve the behavior and the capacity of the deep beams.

- The deep beams designed based on the STM models yielded ductile behaviour and are mostly failed by flexural mode of failure. This type of failure occurred gradually and most of the section capacity is exhausted before failure.
- It seems that the tied arch and arching action controlled the proposed hybrid model. Thus, it is clear that using of lightweight concrete in the lower chord of the deep beam resulted in failure loads of 110% and 104% times that of conventional hybrid deep beam. More economic with less weights would be obtained.
- Using the arched hybrid model shifted the behavior to be more ductile and change the mode of failure from being flexural-shear failure to flexural failure. The crushing at supports was eliminated and cracking occurred within the arch of the lightweight concrete.
- For the horizontal hybrid model of hybridization, toughness enhanced (relative to the non-hybrid beam) by 28% and 143.7% under loading systems of one and two points, respectively. The respective values for arched hybrid model are 65.5% and 144.3% respectively.
- For the loading systems of one point and two points, Ductility increased by 6.6% and 32.5% respectively for the horizontal hybrid deep beam. While the enhancements are 12% and 37.4% respectively for the arched hybrid deep beam.
- Regarding effective stiffness, enhancements of 5.5% and 6.3% (relative to that of the non-hybrid beams) under one-and two points loading systems. Thus may encourage to develop more economic hybrid deep beams that are based on using relatively weak and light concrete out of the path of load transfer

Nomenclatures

d	Diagonal crack width, mm
Eel	Predicted energy, kN.mm
Etot	The total energy dissipated up to failure, kN.mm
f	Flexural crack width, mm

Ke	The effective stiffness, kN/mm
Pcr	Cracking load, kN
Pu	Failure load, kN
Δ ult	Deflection at failure, mm
Δ0.75*Pu*	The deflection at the load level (0.75 Pu), mm

Specimen designations

CTRL-1P	Control deep beam under one point load.
CTRL-2P	Control deep beam under two point load
G1-SN-1P	Horizontal hybrid deep beam under one point load
G1-SN-2P	Horizontal hybrid deep beam under two point load
G2-SL-1P	Arched hybrid deep beam under one point load
G2-SL-2P	Arched hybrid deep beam under two point load

Abbreviations

STM	Strut and tie model
SCC	Self-Compacting Concrete
NC	Normal concrete
SFC	Steel fibers concrete
LWC	Lightweight concrete

References

1. ACI318-19 Committee, (2019). Building code requirements for concrete and commentary, 628.
2. Chen, H. ;Yi, W.-J. ; and Zhou, K.-J. (2022). Diagonal tension cracking strength and risk of RC deep beams. *Buildings*, 12(6), 755, 1-12.
3. Dang, T.D.; Tran, D.T.; Nguyen-Minh, L.; and Nassif, A.Y. (2021). Shear resistant capacity of steel fibres reinforced concrete deep beams: An experimental investigation and a new prediction model. *Structures*, 33, 2284-2300.
4. Shakir, Q.M.; and Hamad, S.A. (2021). Behavior of pocket-type high-strength RC beams without or with dapped ends. *Practice Periodical on Structural Design and Construction*, 26(4), 04021048.
5. Shakir, Q.M.; and Abdlsaheb, S.D. (2022). Rehabilitation of partially damaged high strength RC corbels by EB FRP composites and NSM steel bars. *Structures*, 38, 652-671.
6. Si, X.-Y. ; Zhang, G.-Y.; Zheng, C.; Xu. C.-Y.; Xu, H.; and Wang Y.-L. (2022). Experimental study on shear behavior of reinforced concrete deep beams with high-strength bars under uniform load. *Structures*, 41, 553-567.
7. Hassan, H.M.; Arab, M.A.E.S.; and el-kassas, A.I. (2019). Behavior of high strength self compacted concrete deep beams with web openings. *Heliyon*, 5(4), e01524.
8. Adinkrah-Appiah, K.; and Adom-Asamoah, M. (2016). Characterization and shear strength prediction of reinforced concrete deep beams. *International Journal of Science and Research* (*IJSR*), 5(3), 1789-1798.
9. Mattock, A.H.; and Chan, T.C. (1979). Design and behavior of dapped-end beams. *PCI Journal*, 24(6), 28-45.

10. Smarzewski, P. (2018). Analysis of failure mechanics in hybrid fibre-reinforced high-performance concrete deep beams with and without openings. *Materials*, 12(1), 101.
11. Chin, S.C.; and Doh, S.I. (2015). Behaviour of reinforced concrete deep beams with openings in the shear zones. *Journal of Engineering and Technology*, 6(1), 60-71.
12. Ibrahim, M.A.; El Thakeb, A.; Mostfa, A.A.; and Kottb, H.A. (2018). Experimental study of new reinforcement details for reinforced concrete deep beams with shear opening. *Al-Azhar University Civil Engineering Research Magazine* (*CERM*), 40(1), 347-367.
13. Hamad, S.A.; and Shakir, Q.M. (2021). Behaviour of RC Beams with strengthened web openings under vertical loads. *IOP Conference Series: Materials Science and Engineering*, 1094, 012062, 1-13.
14. Punnoose, S.M.; and Hameed, A.S. (2016). Experimental study of strengthening of RC deep beam with web opening. *International Journal of Innovative Research In Technology*, 3(4), 206-211.
15. Saeed, J.A.; and Yousif, A.R. (2013). Tests of fibrous and nonfibrous reinforced concrete continuous deep beams with web openings. *Journal of Zankoy Sulaimani- Part A* (*JZS-A*), 15 (2), 1-20.
16. Shakir, Q.M. Yahya, Y.M.; and Jasim, A.T. (2019). Strengthening of reinforced self-compacting concrete T- deep beam with large opening by carbon fiber sheets. *Kufa Journal of Engineering*, 10(2), 76-89.
17. Rahim, N.I.; Mohammed, B.S.; Al-Fakih, A.; Wahab, M.M.A.; Liew, M.S.; Anwar, A.; and Amran, Y.H.M. (2020). Strengthening the structural behavior of web openings in RC deep beam using CFRP. *Materials*, 13(12), 2084.
18. Ali, A.A.M.; and Lazim, H.R. (2016). Experimental study of the behavior of deep beams using light-weight structural leca concrete. *International Journal of Innovative Research in Science, Engineering and Technology*, 5(1), 428-436.
19. Fahmi, H.M.; AlShaarbaf, I.A.S.; and Ahmed, A.S. (2013). Behavior of reactive powder concrete deep beams. *AL-Mansour Journal*, 20, special issue, 1-22.
20. Hasan, M.J.; and Al-Shamaa, M.F.K. (2018). Effect bubbles on the behavior of reinforced reactive powder concrete deep beams. *International Journal of Civil Engineering and Technology (IJCIET)*, 9(12), 592-602.
21. Lateef, A.M.; and Ahmed, A.L. (2021). Effect of deep beam width on shear behavior produced by normal and ultra-high performance fiber reinforced concrete. *Advances in Mechanics*, 9(3), 817-827.
22. Hassan, F. (2015). Behavior of hybrid deep beams containing ultra high performance and conventional concretes. *Engineering and Technology Journal*, 33(1), 30-50.
23. Hassan, S.A.; and Faroun, G.A.,(2016). Behaviour of hybrid reinforced concrete deep beams under repeated loading. *Civil and Environmental Research*, 8(10), 14-37.
24. Sada, M.J.; and Resan, S.F. (2021). Shear performance of hybrid concrete deep beams of trapezoidal section. *IOP Conference Series: Materials Science and Engineering*, 1067, 012015.
25. Iraqi Specification No. 5 (1984). Portland Cement. Iraq, Baghdad.

26. Iraqi Specification No.45 (1984). Natural sources for gravel that is used in concrete and construction. Iraq, Baghdad.
27. ASTM A 820-06 (2006). Standard specification for steel fibers for fiber reinforced concrete 1, 1-4.
28. ASTM A615/A615M-04. (2004). *Standard specifications for deformed and plane carbon-steel bars for concrete reinforcement*. Annual Book of ASTM Standard.
29. ASTM C494/C494M-13. (2013). *Standard specification for chemical admixtures for concrete*. Annual Book of ASTM Standard.
30. ACI Committee 237R-07 (2007). Self-consolidating concrete. Farmington Hills, Michigan; American Concrete Institute.
31. ASTM C1621/C1621M-14. (2014). *Standard test method for passing ability of self-consolidating concrete by J-ring*. Annual Book of ASTM Standard.
32. ASTM C39/C39M-15a. (2015). *Standard test method for compressive strength of cylindrical test specimens*. Annual Book of ASTM Standard.
33. BS 1881-116. (1983). Method for determination of compressive strength of concrete cubes. British Standards Institute, London.
34. ASTM C496/C496M-11. (2011). *Standard test method for splitting tensile strength of cylindrical concrete specimens*. Annual Book of ASTM Standard.
35. ASTM C469/C469M-14. (2014). *Standard test method for static modulus of elasticity and Poisson's ratio of concrete in compression*. Annual Book of ASTM Standard.
36. Shakir, Q.M.; and Abd, B.B. (2020). Retrofitting of self compacting RC half joints with internal deficiencies by CFRP fabrics. *Jurnal Teknologi*, 82(6), 49-62.
37. Shakir, Q.M. (2022). Behavior of high-performance RC composite corbels with inclined stirrups. *Canadian Journal of Civil Engineering*, 49(1), 18-30.
38. Shakir, Q.M.; and Abdlsaheb, S.D. (2022). Strengthening of the self-compacted reinforced concrete corbels using NSM steel bars and CFRP Sheets techniques. *Journal of Engineering Science and Technology* (*JESTEC*), 17(3), 1764-1780.
39. Park, R. (1988). Ductility evaluation from laboratory and analytical testing. *Proceedings of the 9th World Conference on Earthquake Engineering*, Tokyo-Kyoto, Japan, 605-616.
40. Taerwe, A. (1995). *Structural ductility of concrete beams prestressed with FRP tendons*. In Naaman, A.; and Jeong S. (eds.). (1st ed.). *Non-metallic (FRP) reinforcement for concrete structures*, CRC Press.
41. Shakir, Q.M.; and Alliwe, R. (2021). The behavior of high strength self-compacting reinforced concrete corbels strengthened with NSM steel bars. *International Journal of Advance Science Engineering Information Technology*, 11(2), 663-673.